Supporting Information

van der Meer et al. 10.1073/pnas.1411215111

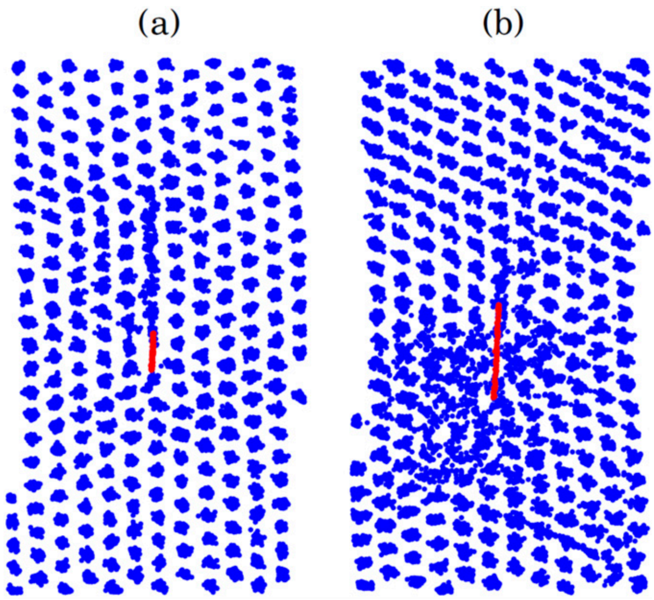

Fig. S1. Experimental particle trajectories (blue) at two different perturbation amplitudes *A* (red) showing two distinct responses. (*A*) For small perturbations $A = 4.9$ µm ($\gamma_L = 0.5$), the crystal responds elastically, whereas (*B*) for higher perturbation amplitudes $A = 12.0$ µm ($\gamma_L = 1.2$), plastic deformation is observed. Lattice spacings: $a \approx 6.3$ µm.

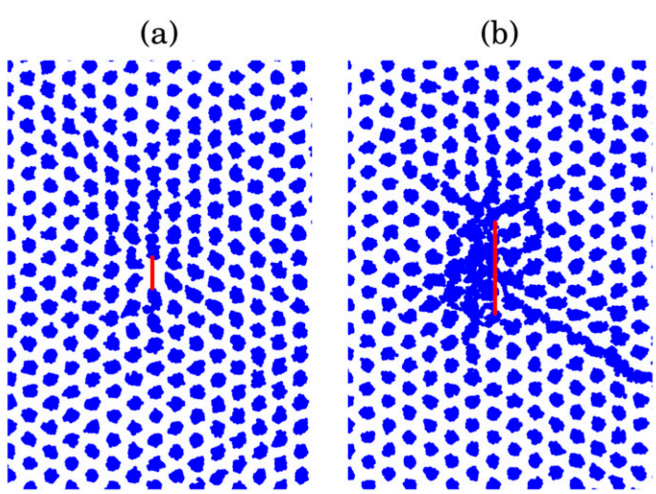

Fig. S2. Simulated particle trajectories (blue) at two different perturbation amplitudes *A* (red) showing two distinct responses. (*A*) For small perturbations $A = 4.0$ µm ($\gamma_L = 0.4$), the crystal responds elastically, whereas (*B*) for higher perturbation amplitudes $A = 12.0$ µm ($\gamma_L = 1.2$), plastic deformation is observed. Lattice spacings: $a \approx 6.3$ µm.

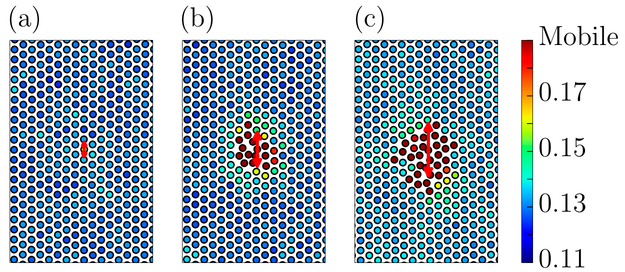

Fig. S3. Color map of the Lindemann parameter L_m showing how the size of the localized mobile region depends on the perturbation amplitude A in simulations. The particles are colored according to their value of the Lindemann parameter L_m and color scale on the right. (*A*) For small amplitudes $A = 2.4$ μm ($\gamma_L = 0.25$), the crystal remains intact, whereas (*B* and *C*) for higher amplitudes $A = 7.2$ ($\gamma_L = 0.7$) and 12.0 μm ($\gamma_L = 1.2$), a localized mobile region surrounds the driven colloid. Lattice spacings: $a \approx 6.3$ μm.

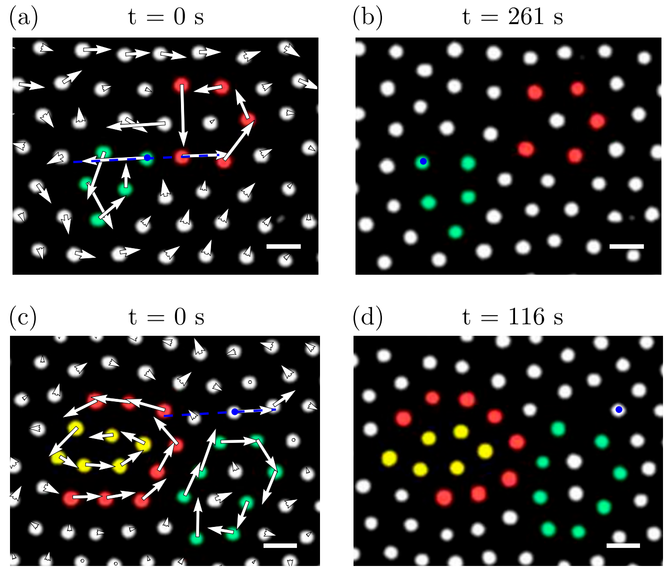

Fig. S4. Bright-field images of various types of string-like rearrangements. The superimposed quivers indicate the particle trajectories. The blue dashed line and dot indicate the path and position of the laser trap, respectively. (*A* and *B*) Initial and final configuration showing two different types of five particle rearrangement loops. The red loop encircles a particle, whereas the green loop does not. Perturbation: $\gamma_L = 1.2$. Note that for this example, the driven particle has experienced 1.3 sinusoidal waves from start to end of the experiment. (*C* and *D*) Initial and final configuration showing an eight- (green) and six- (yellow) particle rearrangement loop. The six-particle loop is partially surrounded by an open string of rearrangements (red). Note that in the final configurations (*B* and *D*) the lattice order has not yet fully restored. These imperfections vanish over time after all rearrangements have completed. Perturbation: $\gamma_L = 1.3$. (Scale bar, 5.0 μm.)

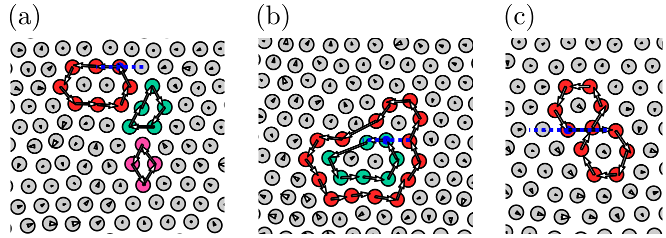

Fig. S5. Simulation snapshots of various types of string-like rearrangements. The superimposed quivers indicate the particle trajectories. The blue dashed line and dot indicate the path and position of the driven particle, respectively. (*A*) Frequently occurring rearrangement loops consisting of four, five, and eight particles ($\gamma_L = 0.8$). (*B*) A 7-particle rearrangement loop that is completely surrounded by a 15-particle rearrangement loop ($\gamma_L = 0.8$). (*C*) An 11-particle rearrangement loop ($\gamma_L = 1.2$).

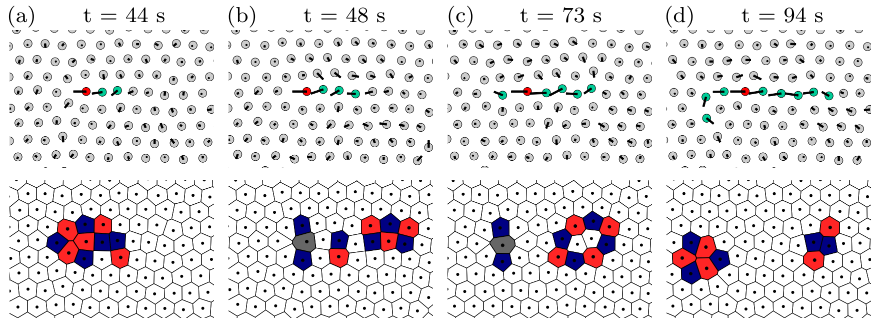

Fig. S6. Time lapse sequence of simulation snapshots and corresponding Voronoi tesselations showing a string of rearrangements, growing from both head and tail for four time steps shown in *A–D*. When the trapped particle (red) is driven along one of the crystal axis, other undriven particles start to move cooperatively as well (green). Perturbation: $\gamma_L = 0.5$.

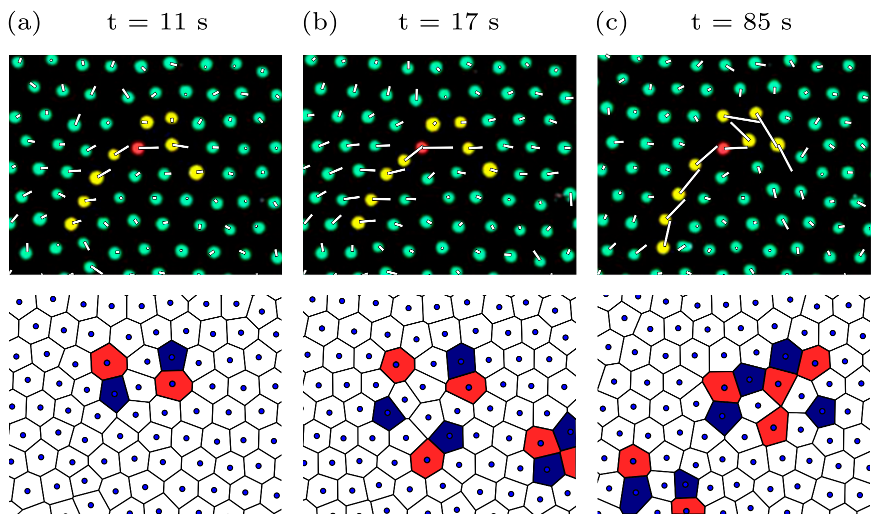

Fig. S7. Time lapse sequence of bright-field images and corresponding Voronoi tesselations showing an open-ended rearrangement string that grows from both head and tail. When the trapped particle (red) is driven along one of the crystal axis, other undriven particles start to move cooperatively as well (yellow). In *A–C*, we superimposed lines that connect the current particle positions with the original equilibrium positions at $t = 0$ s. During the string-like cooperative motion many fivefold (blue) and sevenfold (red) defects are formed. (*A*) In the initial stage of a developing string-like rearrangement, isolated dislocations (isolated 5–7 pairs) are formed. (*B*) One 5–7 pair dissociates into isolated disclinations. The defects at the head of the string perform a gliding motion along with the rearrangement string, driving further cooperative motion, and (*C*) eventually settle into a well-defined interstitial configuration. Perturbation: $\gamma_L = 1.2$. (Scale bar, 5.0 μm.)

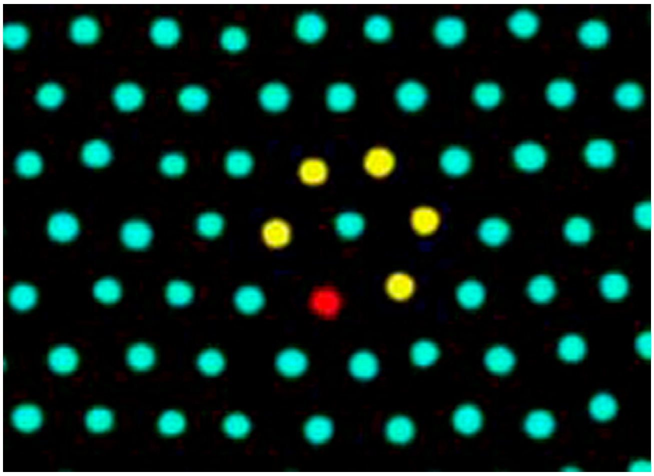

Movie S1. Color-coded bright-field images showing a closed rearrangement loop on the excitation of a single particle. When the trapped particle (red) is driven along one of the crystal axis, other undriven particles start to move cooperatively in a ring-like fashion (yellow). Video sped up by a factor 10.

Movie S1

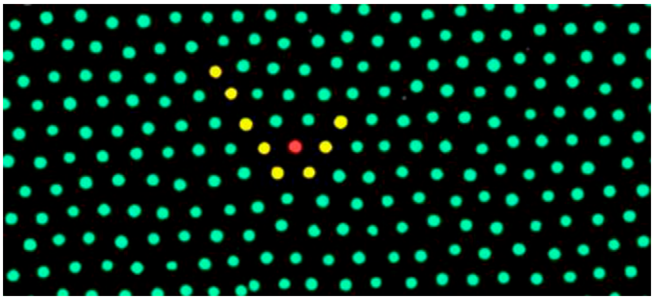

Movie S2. Color-coded bright-field images showing an open-ended rearrangement string that grows from both head and tail on the excitation of a single particle. When the trapped particle (red) is driven along one of the crystal axis, other undriven particles start to move cooperatively as well (yellow). Video sped up by a factor 10.

Movie S2

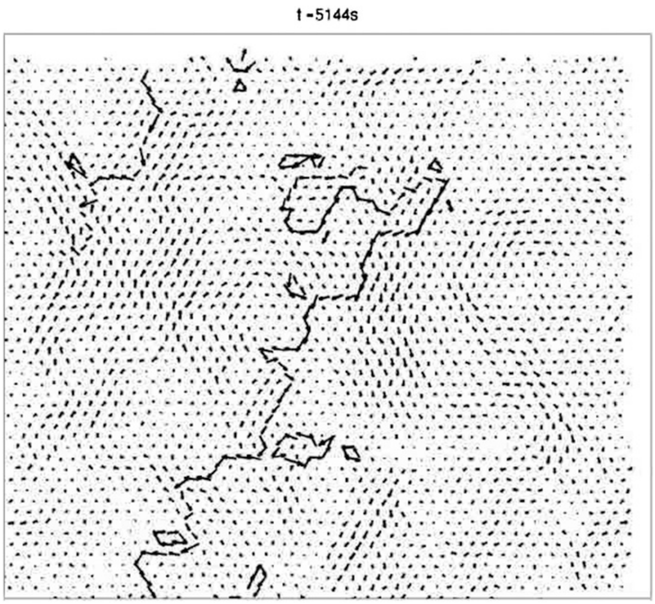

Movie S3. Brownian dynamics simulations showing a spontaneous string of rearrangements occurring through thermal excitation alone. The arrows indicate the displacement of particles with respect to their original lattice positions.

Movie S3